Roughening of a growing surface on a crystal with correlated disorder: Influence of nonlinearity

Sutapa Mukherji
Institut für Theoretische Physik, Universität zu Köln, Zülpicher Strasse 77, D 50937 Köln, Germany
(Received 18 November 1996)

We study the growth of a crystal in the presence of correlated disorder on the substrate. Using a functional renormalization group, we show, for a long-range disorder correlation, an initial decay of the Kardar-Parisi-Zhang-type nonlinearity, though over a large length scale the behavior can be governed by the nonlinearity. [S1063-651X(97)06205-3]

PACS number(s): 05.40.+j, 81.10.Aj, 05.70.Ln, 64.60.Ht

I. INTRODUCTION

The equilibrium shape of a crystal surface undergoes a roughening transition from a rough high-temperature phase to a smooth low-temperature phase as the temperature is decreased [1–3]. Above the roughening transition T_r, the height fluctuations grow logarithmically with the dimension of the system L and below the transition the height is smooth and is independent of L. The nonequilibrium counterpart, the growth mechanism of such crystals, provides more insights about the roughening transition [2]. It is found that for $T>T_r$ the growth is inactivated in nature, whereas for $T<T_r$ the growth is essentially by nucleation of droplets and the growth velocity is exponentially slow in the inverse of the force. For an infinitesimal force F, the mobility that is the ratio of the growth velocity and F vanishes with a jump from a finite value at the transition. With a finite force the transition is blurred. The flat phase is destroyed over a large length scale and eventually becomes rough. In this case a continuous decrease of the mobility is observed as the temperature is lowered [2].

An interesting development in this direction is the inclusion of the disorder of the underlying substrate [4]. The morphology of the growing surface shows a transition that is the super-roughening transition at temperature $T_{\rm sr}$. For $T>T_{\rm sr}$, the height fluctuation is the same as the high-temperature phase of the usual roughening transition, but for $T<T_{\rm sr}$ the surface is rougher than the thermal phase. There is a controversy regarding the roughness of this super-rough phase [5–7] though a recent numerical treatment [8] favors the size dependence of the roughness as $(\ln L)^2$. A dynamical renormalization-group treatment [4] shows that for $T>T_{\rm sr}$ the effect of the disorder essentially vanishes over large length scales and the scaling properties of the surface are the same as that of a surface growing on a pure substrate, in the rough phase. The linear-response mobility in this super-roughening transition vanishes continuously, unlike a jump in the case of the roughening transition, as $T_{\rm sr}$ is approached from the high-temperature phase. For $T<T_{\rm sr}$ there is a temperature-dependent dynamical exponent and a nonlinear response of the system to an external force. The connection between these roughening and super-roughening transitions has been elucidated, furthermore, by a renormalization-group treatment of the growth on a substrate with a correlated disorder [9]. The roughening transition turns into a super-roughening transition as the correlation of the disorder decays sufficiently fast. By tuning the power law of the long-range correlation of the disorder it is possible to go from the pure to the short-range disorder limit.

Such growth problems for crystals need to take into account the periodicity perpendicular to the crystal surface and is usually incorporated in the growth equation by a periodic pinning potential. The low-temperature, flat phase in the roughening transition is due to the relevance of this pinning potential.

The nonequilibrium growth problem is complicated. One has to take into account a relevant nonlinear term that appears due to the lateral growth of an oblique surface [10]. One of the major consequences of this Kardar-Parisi-Zhang (KPZ) nonlinearity is a power-law (not logarithmic) growth of height fluctuations. In the context of the nonequilibrium situation of a crystal surface, it has been argued that with a finite force such a nonlinear term is generated by the interplay of the force and this pinning potential [11]. The asymptotic behavior of the surface might then be determined by the nonlinearity that can destroy the roughening transition. A rough phase can appear even at low temperature. If one starts with a nonlinear term, the lateral growth and the pinning potential combined lead to a phase factor in the pinning potential [12]. This phase factor is also renormalized as one looks at the system over larger length scales. The renormalization of the phase factor makes the identification of the phases a nontrivial problem.

The disorder substrate case is also not well understood. Previous analysis in this direction with a short-range correlation of the disorder of the lattice showed that in the presence of the nonlinearity a small driving force is relevant and the asymptotic properties are essentially governed by the nonlinear term since the finite velocity leads to a smearing of the pinning potential [12]. A numerical investigation, on the other hand, showed a generation of a quenched random mobility [13] and hence a different universality class. The latter has been attributed essentially to the effect of a finite lattice cutoff.

In this paper we address the question of a large-scale description of the dynamics of a growing surface in the presence of a disorder on the underlying lattice and a KPZ-type nonlinearity discussed before. We consider a very general form of the disorder correlation. In view of the conflicting scenario mentioned above, our analysis is based on a renormalization-group technique that involves a finite lattice cutoff. A standard way of describing such a growth phenom-

enon is to start from the equation of motion for the height $\phi(\mathbf{r},t)$ at time t and at coordinate $\mathbf{r}$ in the two-dimensional plane. As mentioned before, the lattice structure orthogonal to the crystal surface is respected through the inclusion of a periodic potential. The equation of motion we need to study is therefore the usual sine-Gordon equation [4,9,11–13] subjected to a constant driving force F,

$$m^{-1}\frac{\partial\phi(\mathbf{r},t)}{\partial t}=K\nabla^2\phi(\mathbf{r},t)-V\sin[\phi(\mathbf{r},t)+d(\mathbf{r})] +\overline{\lambda}/2(\nabla\phi)^2+F+R(\mathbf{r},t), \tag{1}$$

where K denotes the stiffness of the surface, m is the microscopic mobility, and V is the strength of the pinning potential. Here λ represents the strength of the nonlinearity that allows a lateral growth of the surface and R represents the thermal noise at temperature T with a short-range correlation given by

$$\langle R(\mathbf{r},t)R(\mathbf{r}',t')\rangle=(2T/m)\,\delta(\mathbf{r}-\mathbf{r}')\,\delta(t-t'). \tag{2}$$

In the presence of a random substrate we expect that the minima of the periodic potential will be randomly shifted and this is incorporated in this equation through a quenched random variable $d(\mathbf{r})$. We consider here a general form of the correlation associated with this random phase shift $d(\mathbf{r})$, as $g_0\overline{e^{i[d(\mathbf{r})-d(\mathbf{r}')]}}=\gamma(r-r')$, where $g_0=1/2m^2V^2$ and the overbar denotes an average over the disorder. At this point we do not specify the functional form of $\gamma(r-r')$, but later we concentrate on $\gamma(r)\sim r^{-2\alpha}$. We obtain the short-range disorder case for large α and the perfect crystal for $\alpha=0$.

Various limiting forms of this equations that have been studied are as follows. (i) The most well-studied limit is $V=0$ [14]. (ii) The pure equilibrium growth that shows a roughening transition is obtained with $\lambda=F=d=0$ [3,2]. The width of the growing surface is conventionally described by the scaling $w(L,t)=L^{\chi}f(t/L^z)$, where χ is the roughening exponent and z is the dynamical exponent. Above the roughening transition, the width scales as $w(L,t)\sim\ln[Lf(t/L^z)]$, which implies $\chi=0$. In the low-temperature flat phase $w(L,t)$ is independent of L. (iii) The nonequilibrium situation of this pure problem is described by equation 1 with $d=0$, with or without F [11]. (iv) The short-range correlated disorder on the substrate follows from $\gamma(r)=g_0\delta(r)$ [4]. This shows the continuous super-roughening transition. (v) A long-range correlated disorder with $\gamma(r)\sim r^{-2\alpha}$ and $\lambda=0$ shows the interpolation between the roughening and super-roughening transition [9]. Another interesting limit $V=\lambda=0$ and a quenched noise $R(\phi,\mathbf{r})$ were used to study the dynamics of driven interface in a disordered medium [15].

In a renormalization-group (RG) approach the system is looked at on longer length scales by integrating out the effects of small-scale fluctuations. When the system is rescaled to the original scale, the effect of the small-scale fluctuations goes into the renormalization of the various parameters of the problem. The effective coupling constant observed at a certain length scale is then given by the RG recursion relations. In this approach, in all the above cases except (ii), with $F\neq0$, λ has been found not to be renormalized. The important feature that arises in our case is the renormalization of the nonlinearity due to the nonlocal property of the correlator. We obtain a surprising result that this nonlinearity decays initially with the length scale for $F=0$. However, the possible generation of a force and its relevance can cause a truncation of this decay of the nonlinearity and the growth asymptotically becomes KPZ-like. In order to treat the long-range correlation in general, we use the functional renormalization-group (FRG) approach where the renormalization of the correlation function $\gamma(r)$ and its effect on the other parameters are studied.

The paper is organized as follows. Section II is devoted to the description of the effective generating functional. In Sec. III we derive the functional renormalization-group flow equation with necessary diagrams. At this point we might add that our approach is simpler than the dimensional regularization approach of Ref. [12]. Details of the calculations are presented in the Appendixes. Section IV is devoted to the discussion of the asymptotic behavior of the system and connection with previous predictions. In Sec. V we summarize our results.

II. GENERATING FUNCTIONAL

The growth on a crystal substrate with disorder is described by the phase disordered sine-Gordon model with a KPZ nonlinearity as described in Eq. (1). We use the Martin-Siggia-Rose formalism [16] that requires a response field $\tilde{\phi}(\mathbf{r},t)$. Averaging over the disorder [17] yields the generating functional $Z=\int\mathcal{D}\tilde{\phi}\;\mathcal{D}\phi\,\exp[\mathcal{A}]$. Here $\mathcal{A}=\mathcal{A}_0^{(0)}+\mathcal{A}_0^{(d)}$ is the effective action with the free and the disorder part of the action given, respectively, by

$$\mathcal{A}_0^{(0)}=\int dt\;d\mathbf{r}\left\{\frac{1}{2}\vartheta_0\tilde{\phi}_0(\mathbf{r},t)^2-\tilde{\phi}_0(\mathbf{r},t)\left[\mu_0^{-1}\dot{\phi}_0(\mathbf{r},t) -\kappa_0\nabla^2\phi_0(\mathbf{r},t)-\frac{\lambda_0}{2}[\nabla\phi_0(\mathbf{r},t)]^2\right]+\tilde{J}_0(\mathbf{r},t)\tilde{\phi}_0(\mathbf{r},t)\right\}, \tag{3a}$$

$$\mathcal{A}_0^{(d)}=\int dt\;dt'd\mathbf{r}\;d\mathbf{r}'\frac{1}{2}\gamma_0(\mathbf{r}-\mathbf{r}')\tilde{\phi}_0(\mathbf{r},t)\tilde{\phi}_0(\mathbf{r}',t') \times\cos[\phi_0(\mathbf{r},t)-\phi_0(\mathbf{r}',t')], \tag{3b}$$

where $\phi_0=\phi$, $\vartheta_0=2mT$, $\mu_0=1$, $\kappa_0=mK$, $\lambda_0=\overline{\lambda}m$, and $\tilde{J}_0=mF$ are the bare quantities. The Gaussian part of the action [Eq. (3a) with $\lambda_0=0$] gives rise to the following response and the correlation functions [4] in the momentum and frequency representation:

$$\langle\phi(\mathbf{q},\omega)\tilde{\phi}(\mathbf{q}',\omega')\rangle=R(q,\omega)\,\delta(\mathbf{q}+\mathbf{q}')\,\delta(\omega+\omega'),$$

$$\langle\phi(\mathbf{q},\omega)\phi(\mathbf{q}',\omega')\rangle=C(q,\omega)\,\delta(\mathbf{q}+\mathbf{q}')\,\delta(\omega+\omega'), \tag{4}$$

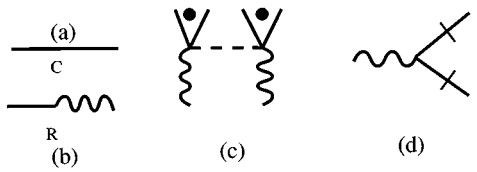

FIG. 1. Diagrammatic representations of (a) the correlation function, (b) the response function, (c) $\tilde{\phi}(\mathbf{r},t)\tilde{\phi}(\mathbf{r}',t')\cos[\phi(\mathbf{r},t)-\phi(\mathbf{r}',t')]$, where dots represent many ϕ lines, and (d) $\tilde{\phi}(\mathbf{r},t)(\nabla\phi)^2$.

where

$$R(q,\omega)=\frac{\mu}{-i\omega+\mu\kappa q^2},$$

$$C(q,\omega)=\frac{\vartheta\mu^2}{\omega^2+\mu^2\kappa^2q^4} \tag{5}$$

(suppressing subscript 0). In the momentum and time representation

$$\langle\phi(\mathbf{q},t)\tilde{\phi}(-\mathbf{q},t')\rangle=\theta(t-t')\mu e^{-\mu\kappa q^2(t-t')},$$

$$\langle\phi(\mathbf{q},t)\phi(-\mathbf{q},t')\rangle=\frac{\mu\vartheta}{2\kappa q^2}e^{-\mu\kappa q^2|t-t'|}, \tag{6}$$

where $\theta(t)=1$ if $t>0$ and zero otherwise. In real space

$$R(\mathbf{r},t)=\frac{\theta(t>0)}{4\pi\kappa t}e^{-r^2/(4\mu\kappa t)}. \tag{7}$$

The correlation function has a divergence due to the long wavelength and for our purpose we define a difference correlation with a suitable ultraviolet regularization introduced by a cutoff Λ as

$$\begin{aligned}Y(|\mathbf{r}-\mathbf{r}'|,t-t')&=\frac{1}{2}\langle[\phi(\mathbf{r},t)-\phi(\mathbf{r}',t')]^2\rangle\\&=\frac{\mu\vartheta}{4\pi\kappa}\int_{|\mathbf{k}|\le\Lambda}\frac{dk}{k}[1-J_0(k|\mathbf{r}-\mathbf{r}'|)\\&\quad\times e^{-\mu\kappa k^2|t-t'|}].\end{aligned} \tag{8}$$

Our analysis involves this difference correlation. The correlation and the response functions are also connected by the fluctuation dissipation theorem (FDT), given as

$$\theta(t>0)\partial_tC(\mathbf{k},t)=-\frac{\mu\vartheta}{2}R(\mathbf{k},t). \tag{9}$$

An important aspect of our system is the breaking of the FDT. This violation of the FDT has previously been argued in the dynamics of random phase sine-Gordon model [18]. The diagrams corresponding to the correlation and response functions are presented in Fig. 1 along with the other two vertices $\tilde{\phi}\tilde{\phi}'\cos(\phi-\phi')$ and $\tilde{\phi}(\nabla\phi)^2$, where $\tilde{\phi}'$ and ϕ' denote the fields at $(\mathbf{r}',t')$. These are the basic diagrams needed for the subsequent perturbative FRG.

III. RENORMALIZATION

In the following we discuss the renormalization scheme to obtain the physics at large distances, which, in the momentum space, corresponds to small $\mathbf{k}$ [19]. We use the description of the fields as sum of the fast and slow modes defined as

$$\begin{aligned}\phi_s&=\phi(k)\quad\text{for}\quad 0<k<\Lambda,\\ \phi_f&=\phi(k)\quad\text{for}\quad \Lambda<k<\Lambda+\delta\Lambda.\end{aligned} \tag{10}$$

This separation of fast and slow modes is used to average out the fast Fourier modes or the short-wavelength details of the problem. These short-wavelength properties are incorporated by the appropriate renormalization of the parameters in the effective action that describes the large length scale properties. By separation of the fast and slow Fourier modes, in general, one arrives at the action

$$\begin{aligned}Z&=\int\prod_{0\le k<\Lambda}\mathcal{D}\phi\,\mathcal{D}\tilde{\phi}e^{\mathcal{A}_0(\phi_s,\tilde{\phi}_s)}\\&\quad\times\int\prod_{\Lambda\le k<\Lambda+\delta\Lambda}\mathcal{D}\phi\,\mathcal{D}\tilde{\phi}\,e^{\mathcal{A}_0(\phi_f,\tilde{\phi}_f)}e^{\mathcal{A}_I(\phi_s,\tilde{\phi}_s,\phi_f,\tilde{\phi}_f)}\\&=\int\mathcal{D}\phi_s\mathcal{D}\tilde{\phi}_se^{\mathcal{A}'(\phi_s,\tilde{\phi}_s)},\end{aligned} \tag{11}$$

where $\mathcal{A}_0$ is the free action and $\mathcal{A}_I$ is the interaction part that contains both fast and slow modes. Here

$$e^{\mathcal{A}'(\phi_s,\tilde{\phi}_s)}=e^{\mathcal{A}_0(\phi_s,\tilde{\phi}_s)}\langle e^{\mathcal{A}_I(\phi_s,\tilde{\phi}_s,\phi_f,\tilde{\phi}_f)}\rangle_{0>}, \tag{12}$$

where $\langle\ \rangle_{0>}$ denotes the average with respect to fast modes of the free action. The next step is a cumulant expansion to clearly identify the contribution from averaging of the fast modes:

$$e^{\mathcal{A}'(\phi_s)}=e^{\mathcal{A}_0+\delta\mathcal{A}}, \tag{13}$$

where

$$\delta\mathcal{A}=\langle\mathcal{A}_I\rangle+(\langle\mathcal{A}_I^2\rangle-\langle\mathcal{A}_I\rangle^2)/2+\cdots.$$

The system in its original length scale is retrieved by rescaling the fields. Rescaling implies that under the transformation $x\to bx$, $t\to b^zt$, $\phi\to b^\chi\phi$ and $\tilde{\phi}\to b^{\tilde{\chi}}\tilde{\phi}$. Around the Gaussian fixed point we have $z=2$, and in a two-dimensional system the rescaling leads to $\tilde{\phi}\to b^{-2}\tilde{\phi}$ with ϕ remaining invariant.

The terms that contribute to the renormalization of various vertices have diagrammatic representations that are presented as we proceed. In the following we consider one-loop diagrams. In fact, in this approach since each internal line in the diagram is within the shell $\Lambda+\delta\Lambda$ it is sufficient to consider the diagrams with only one loop [20]. The effect of the higher loops in the field-theoretic approach [12] is taken care of in our approach by the vertex generated under renormalization. This feeds back to the renormalization of the original vertex that we start with.

The nonlinear term causes a renormalization of the tension κ and the temperature ϑ. We shall not elaborate on this

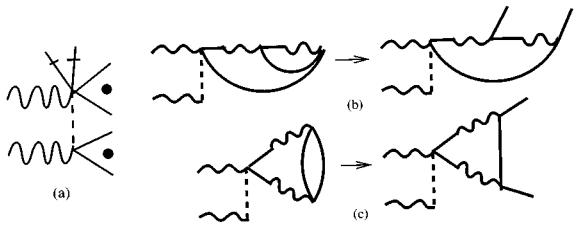

FIG. 2. (a) Vertex $\tilde{\phi}(\mathbf{r},t)\tilde{\phi}(\mathbf{r}',t')[\nabla\phi(\mathbf{r},t)]^2\cos[\phi(\mathbf{r},t)-\phi(\mathbf{r}',t')]$. The hatched line represents $\nabla\phi(\mathbf{r},t)$. (b) and (c) Origin of this vertex. Figures on the left-hand side of the arrows show the two-loop diagrams. The vertex is generated by snipping off one internal line of the two-loop diagram. Diagrams found by this procedure are shown on the right-hand side of the arrows.

part since they are very well documented in previous work [10]. The mobility μ, as well as ϑ and κ, is renormalized by the pinning potential. For local correlator this can be found in Refs. [21,4]. The nonlocality of the correlator requires a more general treatment, which is presented in the Appendix. There is a possible renormalization of the pinning potential due to the nonlinearity. A straightforward diagrammatic expansion would produce two-loop diagrams [12], as shown on the left-hand sides of Figs. 2(b) and Fig. 2(c). To include the effect of these in our RG scheme, we have to involve new vertices whose one-loop contribution would be equivalent to the effect of original diagrams. This vertex, shown in Fig. 2(a), is generated by the combination of λ and $\gamma(r)$ and will be denoted in the following as $\gamma_1(r)$. The explicit form of this vertex is

$$\int dr\, dr'\, dt\, dt'\ \gamma_1(r-r')\tilde{\phi}(\mathbf{r},t)\tilde{\phi}(\mathbf{r}',t') \times\cos[\phi(\mathbf{r},t)-\phi(\mathbf{r}',t')][\nabla\phi(\mathbf{r},t)]^2. \tag{14}$$

It is possible to choose a symmetrized form for this vertex, but the results will remain the same.

The nonlinearity also gets renormalized, unlike the case with a local correlator of Ref. [12]. The diagrams contributing to the renormalization of the nonlinearity is shown in Fig. 3. The details of the derivation of various terms present in the recursion relations are described in the Appendixes. In Appendix A we show the necessary details to find the renormalization of the tension. In Appendixes B and C, the renormalizations of the disorder correlator and the nonlinearity are discussed, respectively. The final flow equations of the parameters in terms of a dimensionless quantity $n_l=\mu\vartheta/8\pi\kappa$ are given as

$$\frac{\partial\kappa}{\partial l}=\frac{1}{8\pi\kappa}\int d\mathbf{r}\, A(r), \tag{15a}$$

$$\frac{\partial\mu^{-1}}{\partial l}=\frac{4n_l}{\mu\vartheta}\int dt\, d\mathbf{r}\, B(r,t), \tag{15b}$$

$$\frac{\partial\vartheta}{\partial l}=4n_l\int d\mathbf{r}\, dt\, B(r,t)+\frac{\lambda^2\mu\vartheta^2}{16\kappa^3(2\pi)}, \tag{15c}$$

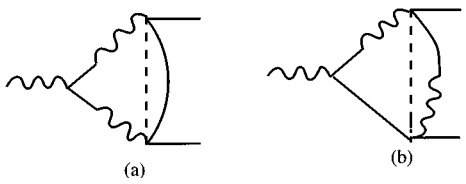

FIG. 3. Diagrams contributing to the renormalization of λ.

$$\frac{\partial\gamma(r)}{\partial l}=(4+\mathbf{r}\cdot\nabla)\gamma(r)-2n_l[\gamma(r)-2\Lambda^2\gamma_1(r)], \tag{15d}$$

$$\frac{\partial\gamma_1(r)}{\partial l}=(2+\mathbf{r}\cdot\nabla)\gamma_1(r)-\frac{n_l\lambda^2}{64\kappa^2\Lambda^2}[\gamma(r)-4\gamma_1(r)\Lambda^2], \tag{15e}$$

$$\frac{\partial\lambda}{\partial l}=-\frac{\lambda}{16\pi\kappa^2}\int d\mathbf{r}\, A(r), \tag{15f}$$

$$\frac{\partial\tilde{J}}{\partial l}=2\tilde{J}+n_l\lambda, \tag{15g}$$

where $A(r)=\gamma(r)r^2J_0(\Lambda r)e^{-Y(r,0)}$ and $B(r,t)=\gamma(r)J_0(\Lambda r)e^{-\mu\kappa\Lambda^2 t}e^{-Y(r,t)}$. The flow equation for γ in this form apparently differs from that of Ref. [12] for a short-range correlation. They obtain a λ-dependent contribution, which in our formulation appears through a vertex γ_1 generated under renormalization. Since $\gamma_1=0$ is the initial condition, one can write, for simplicity, the flow of γ as

$$\frac{\partial\gamma(r)}{\partial l}=(4+\mathbf{r}\cdot\nabla)\gamma(r)-2n_l\gamma(r)-C\lambda^2\gamma(r), \tag{16}$$

where C is a constant, as it is in Ref. [12].

IV. DISCUSSION

For $\lambda=0$, the growth equation, Eq. (1), corresponds to the equilibrium problem [9]. In this case, we recover the equations of Ref. [9]. The recursion relation for the correlator of the form $\gamma(r)\sim c_0r^{-2\alpha}$ for large r implies that α remains unchanged under renormalization, as has been observed in Ref. [9]. It is only the amplitude c_0 that is renormalized. It is also apparent from Eq. (15d) that for $\lambda=0$ the relevance or irrelevance of $\gamma(r)$ is determined by the value of n_l, which plays the role of temperature. For a perfect crystal with $\gamma(r)=g_0$, $n_l=2$ determines the roughening transition, whereas for short-range disorder $\gamma(r)=g_0\delta(r)$, this boundary is at $n_l=1$ [4,9].

For $\gamma(r)=g_0\delta(r)$ the flow equation shows that λ is invariant under renormalization. This is in agreement with Ref. [12]. For any other short-range form of $\gamma(r)$ [e.g., exponentially decaying $\gamma(r)$], it is possible to see from Eq. (16), that the width of the correlation defined as $\int dr\, r^2\gamma(r)/\int\gamma(r)dr$ vanishes as one approaches $l\to\infty$. Interestingly, for a long-range form of $\gamma(r)$, as mentioned above, the integral converges for $\alpha>1$. This $\alpha=1$ is the borderline for the roughening and super-roughening transition [9]. We therefore conclude that any short-range form of $\gamma(r)$ leads to the same conclusion as Ref. [12], namely, that the large-scale

behavior of the growing surface is KPZ-like and the super-roughening transition is lost. With a power-law correlation of the disorder, this short-range limit is achieved when $\alpha>1$.

Let us now consider $0<\alpha<1$. Note that the integral over r in the flow equation for λ is the same as that in the flow equation for κ. Therefore, with $\gamma(r)\sim c_0 r^{-2\alpha}$, this integral is positive as long as $n>5/4-\alpha$ as in Ref. [9]. As a consequence of this, the nonlinearity decreases with the length scale. This is quite an astonishing feature arising due to the nonlocality of the correlator. Recall that the λ term occurs to take into account the lateral growth of the surface. Our result suggests that at least at the initial stage, the lateral growth of the evolving surface is inhibited by the long-distance correlation of the quenched substrate disorder. The effect of this decrease of λ implies that the super-roughening transition is unaffected up to the length scale below which our treatment with $F\to 0$ is valid. If we stop at this leading order of the flow equations, then from [9] we can argue that for $\alpha<1$ one would observe roughening transition. There is, however, a possibility of generation of a driving force due to the nonlinearity λ as given in the recursion relation (15g). The growth of this force with the length scale requires a nonperturbative treatment of the force [11] (explained below) and the decay of the nonlinearity is eventually prevented. The relevant length scale at which this crossover takes place can be obtained by solving the coupled differential equation with and without the force term. Also note that, to this order, the flow of λ and κ, under renormalization, has an invariance $\lambda\kappa^{1/2}=\text{const}$, the physical origin of which is not clear to us.

Let us consider a finite force case. According to Ref. [11], a finite force for a perfect crystal ($\alpha=0$) implies a rough surface with the height fluctuations having a power law scaling with the length. To treat a finite force we redefine the height as

$$\phi(\mathbf{r},t)\to\phi(\mathbf{r},t)+Ft,$$

where F is the external force. This implies a replacement of the disorder part of the action as

$$\mathcal{A}_0^{(d)}=\int dt\ dt'd\mathbf{r}\ d\mathbf{r}'\frac{1}{2}\gamma_0(\mathbf{r}-\mathbf{r}')\tilde{\phi}_0(\mathbf{r},t)\tilde{\phi}_0(\mathbf{r}',t') \times\cos[\phi_0(\mathbf{r},t)-\phi_0(\mathbf{r}',t')+(t-t')F]. \quad (17)$$

The next step is the splitting of cosine into a product of sine and cosine terms. Most crucial is the renormalization of λ, which follows from the possible contraction of the term $\sin[\phi_0(\mathbf{r},t)-\phi_0(\mathbf{r}',t')]\sin[(t-t')F]$. This leads to the flow equation for λ analogous to that in Ref. [11]. We do not go into further details of the calculation since the procedure for extracting this term is similar to the details given in the Appendixes.

The connection with Ref. [13] can also be understood in our approach. There the equation of motion contains a random force. The generating functional obtained after averaging over this random force is in fact the first term of Eq. (3b) in the expansion of the periodic cosine function. The random lateral drift velocity, as suggested in Ref. [13], appears through a vertex similar to γ_1 of Eq. (14) again as a first term in the expansion of the periodic function. The only difference is that there the two $\nabla\phi$ legs are nonlocal in time unlike γ_1 here. The random part of the KPZ nonlinearity is not present in our work, but it will obviously be generated in higher order of λ contributions. In other words, the terms that have been discussed in Ref. [13] are naturally generated or present as the leading-order terms in our functional renormalization scheme with a finite cutoff, though they do not occur in the dimensional regularization scheme of Ref. [12]. We have treated the periodic function completely. It is clear from Sec. III that our renormalization is crucially dependent on the periodic function and, in fact, truncation to first order of the cosine will never lead to any renormalization of λ. Similarly, the finite force scheme is also dependent on the periodic function. We are therefore not sure whether the leading-order terms in the expansion of the cosine function of Eqs. (3b) and (14) can capture the whole effect, especially the question of a different universality class. To address this question one has to go to higher orders in the RG. This remains to be done.

V. SUMMARY

In this paper we investigated the super-roughening transition in the presence of a nonlinearity supporting a lateral growth of the surface. The disorder is considered to have a long-range correlation as discussed after Eq. (2). A functional renormalization-group analysis using a finite momentum cutoff leads to flow equations for the parameters of the growing surface described by Eqs. (1) and (3b), and a flow equation for the disorder correlation. These equations (15a)–(15g) predict the macroscopic properties of the surface. Our equations reduce to the known form of Ref. [12] for short-range correlation of the disorder. The lateral growth governed by the nonlinear term with coefficient λ is initially suppressed due to the long-range disorder correlation. This is apparent from Eq. (15f). Therefore, at least at the initial stage one might expect to see that the super-roughening transition remains unaffected. Over a large length scale a finite force can ultimately lead to a rough surface and destroy the transition. This requires a treatment of a finite force as discussed in Sec. IV. In our analysis, we have taken a finite cutoff and have shown that the terms that have been predicted from numerical lattice simulations are really generated, though our analysis envisages a more general term.

ACKNOWLEDGMENTS

I thank S. Scheidl for introducing me to this field. I also thank T. Nattermann and S. M. Bhattacharjee for various useful comments. Support from SFB 341 is acknowledged.

APPENDIX A: RENORMALIZATION OF THE TENSION

We discuss only the contribution of the pinning potential $\gamma(r)$ to the renormalization of the tension κ. The renormalization of the other quantities such as temperature and mobility can be found out in an analogous way with appropriate diagrams. One representative Feynman diagram that contributes to the renormalization of the tension is shown in Fig. 4. The external lines are associated with momentum $\mathbf{K}$ and all the internal lines contain fast momenta. However, the sum of all of the internal momenta should add up to yield K. Let us choose one internal C line with momentum Λ as shown in Fig. 4. Its contribution in real space is

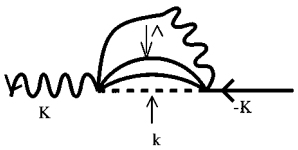

FIG. 4. Diagram contributing to the renormalization of the tension κ.

$$\int d\mathbf{p}\ \Lambda\delta(p-\Lambda)\exp(i\mathbf{p}\cdot\mathbf{r})C(p,t) = \frac{\Lambda^2}{2\pi}J_0(\Lambda r)\frac{\mu\vartheta}{2\kappa\Lambda^2}\exp(-\mu\kappa\Lambda^2|t|)\equiv G^{\phi,\phi}(r,t). \tag{A1}$$

Therefore, the contribution of Fig. 4 is

$$\frac{1}{2}\int dt \int d\mathbf{r}\int d\mathbf{k}\ \exp[-i(\mathbf{K}-\mathbf{k})\cdot\mathbf{r}]G^{\phi\phi}(r,t)R(r,t) \times\exp[-Y(r,t)]\gamma(k), \tag{A2}$$

where $\exp[-Y(r,t)]$ takes care of the sum over all possible diagrams that arise from all possible contractions of the internal lines, as it is in the case of the local correlator [4,12]. The other possibility arises when one associates the R line with the momentum Λ. In this case we have the line with the fast momentum as

$$\int d\mathbf{p}\ \Lambda\delta(p-\Lambda)\exp(i\mathbf{p}\cdot\mathbf{r})R_0(p,t) = \frac{\Lambda^2}{2\pi}J_0(\Lambda r)\mu e^{-\mu\kappa\Lambda^2 t}\equiv G^{\phi,\tilde{\phi}}(r,t) \tag{A3}$$

and the full expression is

$$\frac{1}{2}\int dt \int d\mathbf{r}\int d\mathbf{k}\ \exp[-i(\mathbf{K}-\mathbf{k})\cdot\mathbf{r}]G^{\phi\tilde{\phi}}(r,t) \times\exp[-Y(r,t)]\gamma(k). \tag{A4}$$

The flow equation for the tension is obtained by addition of Eqs. (A4) and (A2) with an extra symmetry factor, completing the integral over $\mathbf{k}$ and extracting the term proportional to K^2. The simplified form given in Eq. (15a) is achieved by the use of the FDT and a subsequent integration by parts over t.

APPENDIX B: RENORMALIZATION OF γ

The first term in the flow equation of γ is, in fact, the result of the contribution that comes from expanding the cosine in the pinning potential. The simplest diagram in the one loop level is shown in Fig. 5. The corresponding expression is

$$\frac{\gamma(r)}{2}\int\frac{d\mathbf{k}}{(2\pi)^2}\Lambda\delta(k-\Lambda)C(k,0). \tag{B1}$$

This leads to the first term of the RG contribution in Eq. (15d). The second term with γ_1 in Eq. (15d) will be clear from the following discussion. The contribution that comes from the combined effect of the nonlinearity is at the two-loop level and the possible diagrams are shown explicitly in Ref. [12]. The effect of these diagrams is incorporated through a higher-order vertex. The usual procedure that is adopted is to snip off the internal line [22] and generate another vertex. This vertex will renormalize the vertex γ when they are rejoined again. We pick up one such two-loop diagram that contributes in the field-theoretic approach. Snipping off one internal line leads to a vertex of the form given in Eq. (14).

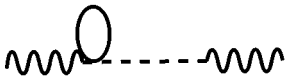

FIG. 5. Diagram contributing to the renormalization of γ.

We call this vertex $\gamma_1(r)$, which differs from the $\gamma(r)$ vertex by two $\nabla\phi$-type legs. Once they are rejoined this vertex will contribute to renormalization of $\gamma(r)$. The second term with γ_1 in Eq. (15d) follows from this prescription. We now discuss the renormalization of the vertex γ_1. There are two such possible diagrams that can originate from the original two-loop diagrams and lead to the renormalization of γ_1. From the other two-loop diagrams it is easy to observe that no such vertex that respects the symmetry of the system can be formed. The contribution of the γ_1 vertex in the renormalization of γ is identical to the contribution of the γ vertex itself, except for a multiplicative factor Λ^2, which is obvious from a dimensional analysis. As it is evident from Fig. 2, this vertex is generated from the term of $O(\lambda^2\gamma)$. It is easy to evaluate the expressions of the diagrams in Fig. 2. In the momentum and frequency representation, Fig. 2(b) can be expressed as

$$-\frac{\lambda^2}{4}\gamma(r)\int_0^\infty dt_2\int_0^{t_2}dt_1\int dk_2 R(k_{2m1},t_2-t_1) \times C(k_{2m1},t_2)R(k_{2p1},t_1)(\mathbf{k}_1\cdot\mathbf{k}_{2p1})(\mathbf{k}_1\cdot\mathbf{k}_{2m1}) = -\frac{\mu\vartheta}{8\pi\kappa}\frac{\lambda^2}{16\kappa^2\Lambda^2}\frac{\gamma(r)}{4}k_1^2, \tag{B2}$$

where $\mathbf{k}_{2p1}=\mathbf{k}_2+\mathbf{k}_1/2$ and $\mathbf{k}_{2m1}=\mathbf{k}_2-\mathbf{k}_1/2$ in the hydrodynamic limit, i.e., $k_1\to 0$. Similarly, the contribution from Fig. 2(c) is

$$\frac{\mu\vartheta}{8\pi\kappa}\frac{\lambda^2}{8\kappa^2\Lambda^2}\frac{\gamma(r)}{4}k_1^2. \tag{B3}$$

A similar contribution comes from the vertex involving γ_1. The combined expression leads to the recursion relation for γ_1 in Eq. (15e). The vertex γ_1 is completely the effect of renormalization.

APPENDIX C: RENORMALIZATION OF λ

We notice that the possible one-loop diagrams that contribute to the renormalization of the nonlinearity λ in the case of the nonlocal correlator are those shown in Fig. 3. There are other possible diagrams that could lead to a con-

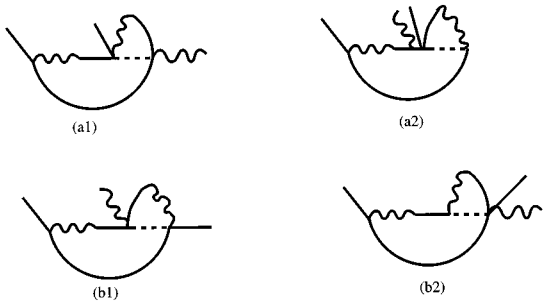

FIG. 6. Diagrams that could contribute to the renormalization of λ, but vanish due to their mutual cancellation.

tribution in the renormalization of the nonlinearity. But we note that they cancel altogether, for example, the diagrams shown in Fig. 6. The expression corresponding to the diagram in Fig. 3(a) is

$$-\frac{\lambda}{4}\int \frac{d\mathbf{k}_1}{(2\pi)^2} d\omega_1 R(k_1,\omega_1)R(k_1,-\omega_1) \times \int d\mathbf{r}\int_0^\infty dt\ \gamma(r)\ \frac{k_1^2 r^2}{2} e^{-Y(r,t)} e^{i\mathbf{k}_1\cdot\mathbf{r}} e^{-i\omega_1 t}. \tag{C1}$$

After the integration over the shell momentum k_1 we obtain the contribution of Fig. 3(a) as

$$-\frac{\mu^2\lambda\Lambda^4}{32\pi^2}\int d\omega_1 \frac{1}{(\mu\kappa\Lambda^2)^2+\omega_1^4} \times\int_0^\infty dt\int d\mathbf{r}\ \gamma(r) r^2 J_0(\Lambda r) e^{i\omega_1 t} e^{-Y(r,t)}.$$

Furthermore, the integration over the frequency leads to the final contribution of Fig. 3(a) as

$$-\frac{\mu\lambda\Lambda^2}{32\pi\kappa}\int_0^\infty dt\ d\mathbf{r}\ r^2\gamma(r) J_0(\Lambda r) e^{-Y(r,t)} e^{-\mu\kappa\Lambda^2 t}. \tag{C2}$$

Similarly, the expression corresponding to Fig. 3(b) is

$$-\frac{\lambda}{16}\int \frac{d\mathbf{k}_1}{(2\pi)^2}\ d\omega_1 R(k_1,\omega_1)C(k_1,\omega_1) \times\int d\mathbf{r}\int_0^\infty dt\ r^2 R(r,t)\gamma(r) k_1^2 r^2 e^{i\omega_1 t} e^{-Y(r,t)}. \tag{C3}$$

After performing the integration over the momentum shell and the frequency, we get for Fig. 3(b),

$$-\frac{\lambda\vartheta\mu}{128\pi\kappa^2}\int d\mathbf{r}\int_0^\infty dt\ r^2\gamma(r)R(r,t)J_0(\Lambda r) e^{-\mu\kappa\Lambda^2 t} e^{-Y(r,t)}. \tag{C4}$$

Use of the relation

$$\theta(t>0)\partial_t e^{-Y(r,t)} = -\frac{\mu\vartheta}{2} R(r,t) e^{-Y(r,t)} \tag{C5}$$

and subsequent integration over t leads to the following expression for Fig. 3(b):

$$-\frac{\lambda}{64\pi\kappa^2}\int d\mathbf{r}\ r^2 J_0(\Lambda r)\gamma(r) e^{-Y(r,0)} + \frac{\lambda\mu\Lambda^2}{64\pi\kappa}\int d\mathbf{r}\int_0^\infty dt\ r^2 J_0(\Lambda r)\gamma(r) e^{-Y(r,t)} e^{-\mu\kappa\Lambda^2 t}. \tag{C6}$$

Combining the contributions of Figs. 3(a) and 3(b) with the appropriate symmetry factor, we arrive at the recursion relation for λ.

The diagrams in Fig. 6 can be evaluated in a similar manner. The expression for Fig. 6(a1) is

$$\int \frac{d\mathbf{k}}{(2\pi)^2}\int d\omega\ R(p_+,\omega)C(p_-,\omega)\mathbf{p}\cdot\mathbf{p}_- \times\int d\mathbf{r}\int_0^\infty dt\ \gamma(r)R(r,t)J_0(p_- r) e^{-Y(r,t)} e^{i\omega t} \tag{C7}$$

and for Fig. 6(b1) is

$$\int \frac{d\mathbf{k}}{(2\pi)^2}\int d\omega\ R(p_+,\omega)C(p_-,\omega)\mathbf{p}\cdot\mathbf{p}_- \times\int d\mathbf{r}\int_0^\infty dt\ \gamma(r)R(r,t) e^{-i\omega t} e^{-Y(r,t)} J_0(p_+ r), \tag{C8}$$

where $\mathbf{p}_+ = \mathbf{p}/2+\mathbf{k}$ and $\mathbf{p}_- = \mathbf{p}/2-\mathbf{k}$. In the above equations $\mathbf{p}$ is the slow momentum and the contribution to the λ vertex can arise from the following terms after adding Figs. 6(a1) and 6(b1):

$$\int d\mathbf{r}\int_0^\infty dt\ \gamma(r)J_0(\Lambda r)R(r,t)e^{-Y(r,t)}\ \int\frac{d\mathbf{k}}{(2\pi)^2}2p_+^2 \times\mathbf{p}\cdot(\mathbf{p}/2-\mathbf{k})\int d\omega\ e^{i\omega t}\frac{1}{(p_+^4+\omega^2)(p_-^4+\omega^2)} + \int d\mathbf{r}\int_0^\infty dt\ r\ \gamma(r)J_0(\Lambda r)R(r,t)e^{-Y(r,t)}\int\frac{d\mathbf{k}}{(2\pi)^2} \times\mathbf{p}\cdot(\mathbf{p}/2-\mathbf{k})\int d\omega\ e^{i\omega t}\frac{\mathbf{p}\cdot\mathbf{k}(-2i\omega)}{(p_+^4+\omega^2)(p_-^4+\omega^2)}. \tag{C9}$$

We need not go into the final expression corresponding to the combined contribution of Figs. 6(a1) and 6(b1). This is because, interestingly, the other two diagrams in Figs. 6(a2) and 6(b2) lead to the same contribution but *with opposite sign*, thereby canceling the contribution of Figs. 6(a1) and 6(b1). This cancellation leads to a considerable simplification of the recursion relations.

[1] H. van Beijeren and I. Nolden, in *Structure and Dynamics of Surfaces II*, edited by W. Schommers and P. von Blanckenhagen (Springer, Berlin, 1987).
[2] P. Noziers and F. Gallet, J. Phys. (Paris) **48**, 353 (1987); P. Noziers, in *Solids far from Equilibrium*, edited by C. Godreche (Cambridge University Press, Cambridge, England, 1992).
[3] S. T Chui and J. D. Weeks, Phys. Rev. Lett. **38**, 4978 (1976).
[4] Y.-C. Tsai and Y. Shapir, Phys. Rev. Lett. **69**, 1773 (1992); Phys. Rev. E **50**, 3546 (1994).
[5] J. J. Cardy and S. Ostlund, Phys. Rev. B **25**, 6899 (1982); J. Toner and D. P. Divincenzo, *ibid.* **41**, 632 (1990).
[6] S. E. Korshunov, Phys. Rev. B **48**, 3969 (1993); T. Giamarchi and P. LeDoussal, Phys. Rev. Lett. **72**, 1530 (1994).
[7] D. Cule and Y. Shapir, Phys. Rev. Lett. **74**, 114 (1995); H. Rieger, *ibid.* **74**, 4964 (1995).
[8] C. Zeng, A. A. Middleton, and Y. Shapir, Phys. Rev. Lett. **77**, 3204 (1996); H. Rieger and U. Blasum (unpublished).
[9] S. Scheidl, Phys. Rev. Lett. **75**, 4760 (1995).
[10] M. Kardar, G. Parisi, and Y. C. Zhang, Phys. Rev. Lett. **56**, 889 (1986); E. Medina, T. Hwa, M. Kardar, and Y. C. Zhang, Phys. Rev. A **39**, 3053 (1989).
[11] M. Rost and H. Sphon, Phys. Rev. E **49**, 3709 (1994).
[12] Y.-C. Tsai and Y. Shapir, Phys. Rev. E **50**, 4445 (1994).
[13] J. Krug, Phys. Rev. Lett. **75**, 1795 (1995).
[14] For a recent review, see T. Halpin-Healy and Y.-C. Zhang, Phys. Rep., **254**, 215 (1995).
[15] T. Nattermann, S. Stepanow, L.-H. Tang, and H. Leschhorn, J. Phys. (France) II **2**, 1483 (1992).
[16] P. C. Martin, E. D. Siggia, and H. A. Rose, Phys. Rev. A **8**, 423 (1973).
[17] In this formalism, the generating function describes the probability of the height variable ϕ. We therefore can average the generating function over the disorder.
[18] D. Cule and Y. Shapir, Phys. Rev. B **51**, R3305 (1995).
[19] P. Shukla, in *Models and Techniques of Statistical Physics*, edited by S. M. Bhattacharjee (Narosa, London, 1997).
[20] F. J. Wegner and A. Houghton, Phys. Rev. A **8**, 401 (1973).
[21] Y. Y. Goldschmidt and B. Schaub, Nucl. Phys. B **251**, 77 (1985).
[22] See, e.g., R. Shankar, Rev. Mod. Phys. **66**, 129 (1994).